Opto-Hydrodynamic Tweezers

SHREYAS VASANTHAM[A], ABHAY KOTNALA [AB*], YURII PROMOVYCH[A], PIOTR GARSTECKI[A] , LADISLAV DERZSI[A*]

[A]*Institute of Physical Chemistry, Polish Academy of Sciences, Kasprzaka 44/52, 01-224, Warsaw, Poland*
[B]*Department of Electrical and Computer Engineering, University of Houston, Houston, Texas, 77204*

*akotnala@central.uh.edu
*lderzsi@ichf.edu.pl

Supplementary Information

S1: Experimental set-up of Opto-Hydrodynamic Tweezers

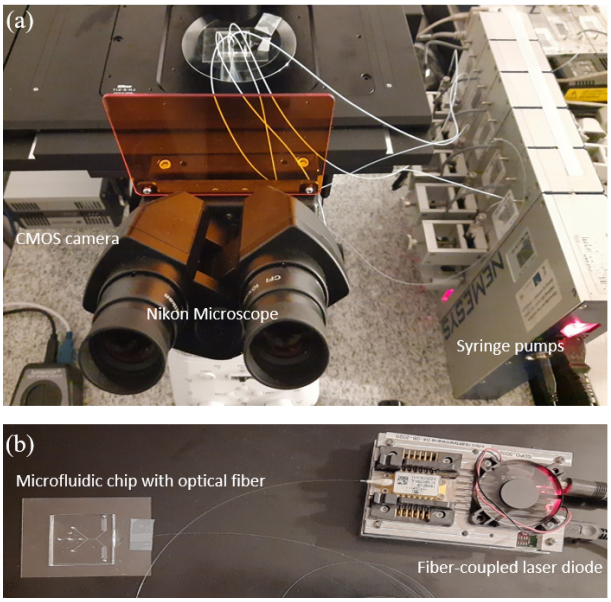

Figure S1: Experimental set-up of the opto-hydrodynamic tweezers (OHT). The microfluidic chip with integrated fiber optics is placed on the inverted microscope and connected to high precision low pressure syringe pumps. The chip with the fiber optics together is of a size of an average cell phone and in a suitable protective case could be carried in one's pocket. The inverted microscope was used only for bright-field imaging of the microfluidic channel. The bulky microscope system can be simply replaced by an imaging lens-camera assembly to build a compact lab-on-chip OHT device.

S2: Calculation of optical forces in OHT

The output beam from the end-face of a single mode fiber was modelled as a single Gaussian beam propagating in a water medium (n=1.33), as the guided fiber mode has near-Gaussian characteristics. The intensity profile of the launched beam from the optical fiber within the channel can be modelled as

$$I(x,y) = I_o \exp\left(\frac{-2y^2}{w(x)^2}\right) = \frac{2P}{\pi {w_o}^2} \exp\left(\frac{-2y^2}{w(x)^2}\right)$$

$$w_o = \frac{MFD}{2}$$

$$w(x) = \frac{MFD}{2}\sqrt{1 + \left(\frac{x}{x_r}\right)^2}, \quad x_r = \frac{\pi}{\lambda}\left(\frac{MFD}{2}\right)^2$$

where, MFD is the mode-field diameter of the optical fiber, I_o is the peak irradiance at the center of the beam, y is the radial distance away from the axis, $w(x)$ is the radius of the laser beam where the irradiance is $1/e^2$ (13.5%) of I_o, x is the distance propagated from the end-face of the fiber, and P is the total power of the beam.

In all of our experiments we used a polarization maintaining photosensitive single mode optical fiber (Thorlabs, USA). For calculations and for profiling the spatial distribution of optical forces (Fig. 2 and Fig. S2) we used the values of the numerical apertures, NA and mode field diameter MFD, from the spec sheet provided by the manufacturer (NA=0.12; MFD@980nm = 6.6 ± 1.0 µm). However, MFD alternatively can also be calculated from the numerical aperture, NA of the optical fiber (and vice-versa), using the simple relation:

$$\theta_{sm} \approx \frac{0.64\lambda}{MFD}$$

where $\theta_{sm} = \sin^{-1} NA$, NA is the numerical aperture of the fiber, θ_{sm} is the divergence or the acceptance angle in radians, λ is the wavelength (973 nm) and MFD is the mode-field diameter.

Figure S2 shows the spatial intensity profile of the laser beam launched from an optical fiber into the microfluidic channel with output optical power of P= 550 mW, *MFD*=6.5 µm and wavelength of λ=973 nm.

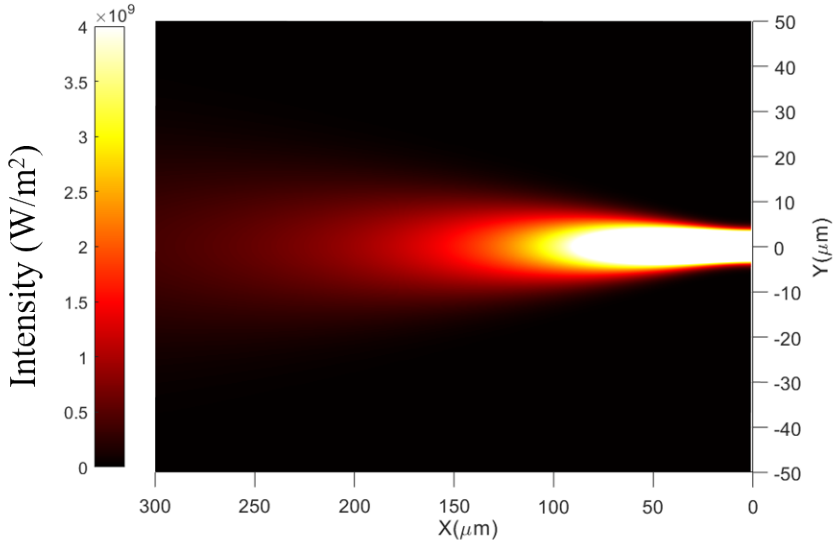

Figure S2: Spatial intensity profile of the laser beam launched from the end face of a single mode optical fiber into the microfluidic channel filled with water. The origin is located at the centre of the core of the fiber.

The optical forces acting on the particle at any given position within the channel is given by

$$F_{scat}(x,y) = \frac{n_m a^2 2\pi}{2c} \int_0^{\frac{\pi}{2}} \int_0^{} I(x,y) Q_{scat} \sin(2\theta_1) d\theta_1 d\varphi$$

$$F_{grad}(x,y) = \frac{-n_m a^2 2\pi}{2c} \int_0^{\frac{\pi}{2}} \int_0^{} I(x,y) Q_{grad} \sin(2\theta_1) cos\varphi d\theta_1 d\varphi$$

, where n_m is the refractive index of the medium, a is the radius of the trapped particle, c is the speed of light. Q_{scat} and Q_{grad} are given by

$$Q_{scat} = \left[1 + Rcos(2\theta_1) - T^2 \frac{cos(2\theta_1 - 2\theta_2) + Rcos(2\theta_1)}{1 + R^2 + 2Rcos(2\theta_2)}\right]$$

$$Q_{grad} = \left[Rsin(2\theta_1) - T^2 \frac{sin(2\theta_1 - 2\theta_2) + Rsin(2\theta_1)}{1 + R^2 + 2Rcos(2\theta_2)}\right]$$

where R and T are the Fresnel reflection and transmission coefficient for optical rays' incident at an angle θ_1. θ_2 is the angle of refraction calculated using Snell's law.

S3: Estimation of non-optical forces in OHT

Buoyant force acting on a rigid spherical particle suspended in a medium is given by

$$F_b = \frac{4}{3}\pi a^3 \rho_m g$$

The gravitational force is given by

$$F_s = \frac{4}{3}\pi a^3 \rho_P g$$

, where ρ_m and ρ_p are the density of the medium and particle respectively, a is the radius of the particle, g is the acceleration due to gravity.

The lift forces are given by[1–3]

Shear-gradient lift forces: $F_{SL} \propto \rho_m \, v^2 \frac{a^3}{H}$

Wall lift forces: $F_{WL} \propto \rho_m \, v^2 \frac{a^6}{H^4}$

where, ρ_m is the density of the medium, v is the maximum velocity, a is the radius of the particle and H is the characteristic dimension of the channel. For rectangular channel,

$$H = \frac{2wh}{(w+h)}$$

, where w and h are the width and height of the channel.

Since 3D hydrodynamic flow focusing ensures that particles are aligned with the optical axis of the fiber, which is close to the centre of the channel (within ± 10 µm) and far away from the channel walls; the magnitude of the inertial lift forces acting on the particle is almost three orders of magnitude smaller than the optical trapping forces in our geometry and therefore do not contribute to the trapping forces.

S4: 3D Hydrodynamic flow focusing

A four-way sheath and sample flow system as demonstrated previously[4], was used for implementing the 3D hydrodynamic flow focusing in the microfluidic channel. Due to the laminar flows in the microfluidic channel (Re << 1), the fluid in the channels flow with no disruption between the layers and without lateral mixing, which forms the basis for 3D hydrodynamic flow focusing. Briefly, the lateral sheath flows from inlet 1 and 2 as shown in Figure 1a of the manuscript, were used to focus the sample flow in the horizontal direction (Y-axis, along the width of the channel). Similarly, the top and bottom sheath flows from inlet 4 and 5 as shown in Figure 1b, were used to compress the sample flow in the vertical direction (Z-axis, along the height of the channel). By properly adjusting the flow rate of the four sheath and sample flows, particle trajectories can be hydrodynamically manipulated within the cross-section of the microfluidic channel. Table S1 shows the sheaths and sample flow rates used in our experiments to align the particle trajectories with the optical axis of the fiber, positioned almost at the centre of the cross-section of the channel. Figure S2 shows the aligned polystyrene particles in the microfluidic channel as they enter into the main channel from the junction (See Supplementary Video S1). It should be noted that the magnitude of the sheath flow rates used to obtain specific particle trajectories within the channel might differ slightly between two experiments or sometimes during the experiments, due to the variations in the pressure difference between the inlets and outlets due to the presence of air bubble or stretching of PDMS etc. Therefore, the sheath flow rates should be optimized each time to obtain the best alignment of particle trajectory with the optical axis of the fiber.

The syringe pumps are initialized at the recommended pulse free limit of 10 µL/hr. The flow rates for top, bottom and sample are kept fixed at 10µL/hr. The overall flow rate on the sides was adjusted from 10 – 100 µL/hr to observe flow of polystyrene particles in a streamlined fashion within the main channel. When flow rate ratios of sample (Q_{sample}) to side sheath (Q_{side}) reached values around 1:5, the particles began to flow in the center of the cross section of the main channel in a queue.

Since the optical fiber is manually inserted into the waveguide channel and the relative position of the fiber core might vary by a few microns. It should be noted that the magnitude of the sheath flow rates used to obtain specific particle trajectories within the channel might differ slightly between two experiments and must be optimized as mentioned above to achieve best alignment of particle trajectory with the optical axis of the fiber.

Table S1: Sheath and sample flow rates used for 3D hydrodynamic flow focusing to align the particle trajectories with the optical fiber axis in the microfluidic channel

Q_{Bottom}	Q_{Sample}	Q_{Top}	Q_{Side} (from both sides)	Width of the focussed stream
10 µL/hr	10 µL/hr	10 µL/hr	10 µL/hr	60 µm

10 µL/hr	10 µL/hr	10 µL/hr	25 µL/hr	20 µm
10 µL/hr	10 µL/hr	10 µL/hr	50 µL/hr	15 µm
10 µL/hr	10 µL/hr	10 µL/hr	75 µL/hr	13 µm
10 µL/hr	10 µL/hr	10 µL/hr	100 µL/hr	6 µm

Changing top and bottom sheath flow to achieve desired focusing along z- axis. Alignment with the optical axis of the trapping fiber.

Table S2: Sheath and sample flow rates used for 3D hydrodynamic flow focusing to align the particle trajectories with the optical fiber axis in the microfluidic channel

Sheath flow 1	**Sheath flow 2**	**Sample flow 3**	**Sheath flow 4**	**Sheath flow 5**
55 µL/Hr	55 µL/Hr	10 µL/Hr	10 µL/Hr	10 µL/Hr

Changing top and bottom sheath flow to achieve desired focusing along z- axis. Alignment with the optical axis of the trapping fiber.

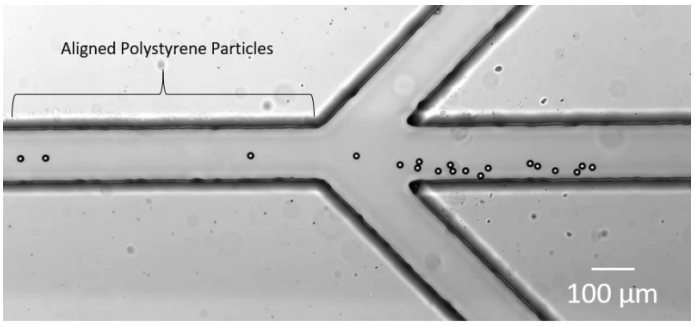

Figure S3: Optical microscope image showing the alignment of the trajectories of polystyrene particles with the centre of the cross-section of the channel using 3D hydrodynamic flow focusing. The microscope objective was focused at the centre of the channel thickness.

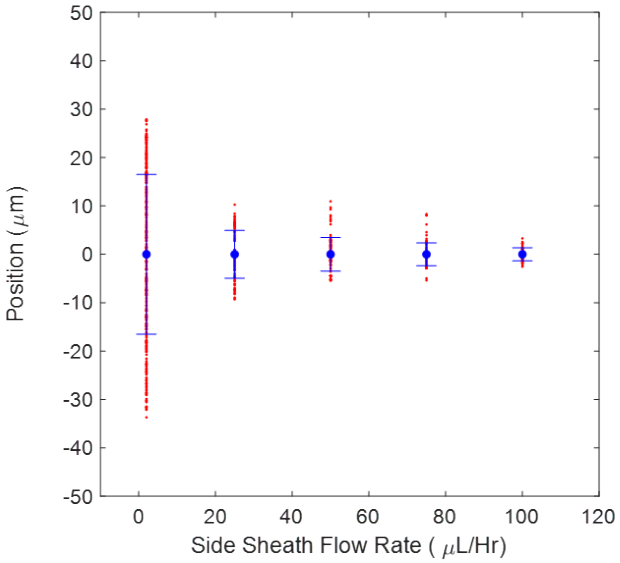

Figure S4: Position (centroid) of the polystyrene beads flowing in the channel along the Y direction, i.e. along the width of the channel after 3D hydrodynamic flow focusing for different side sheath flow rates. Each red dot represents the Y-position of a single particle flowing in the channel. The errorbar represent the mean and standard deviation in the positions.

S5: Trapping of multiple particles as long chains

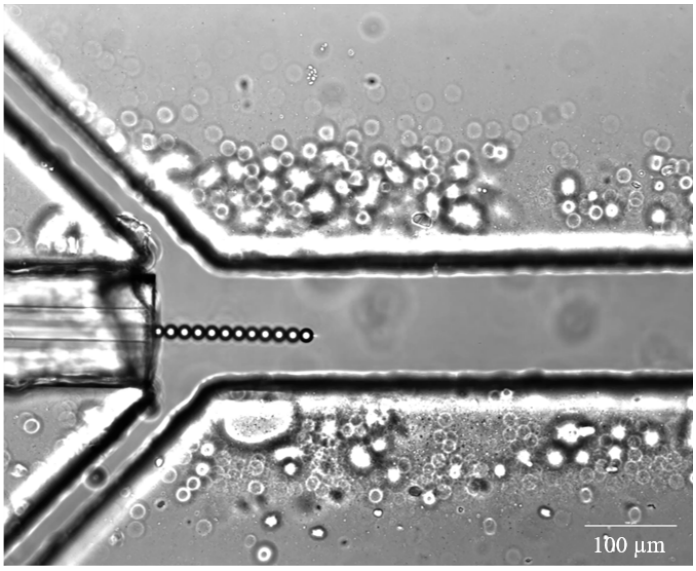

Figure S5: Optical image showing the trapping of multiple particles forming long chain in an opto-hydrodynamic trap. The number of trapped beads in the chain are 12.

S6: Measurement of Flow Velocities in the Microfluidic Channel

The flow velocities in the channel were calculated from the time trajectories of particles flowing within the channel. From the recorded videos, we extracted the positions of the trapped particle (centroid), once it was released from the trap and it flowed along the length of the channel. Figure S6 shows the time trace of the positions of a representative particle flowing in the channel. A linear fit was used to calculate the flow velocity.

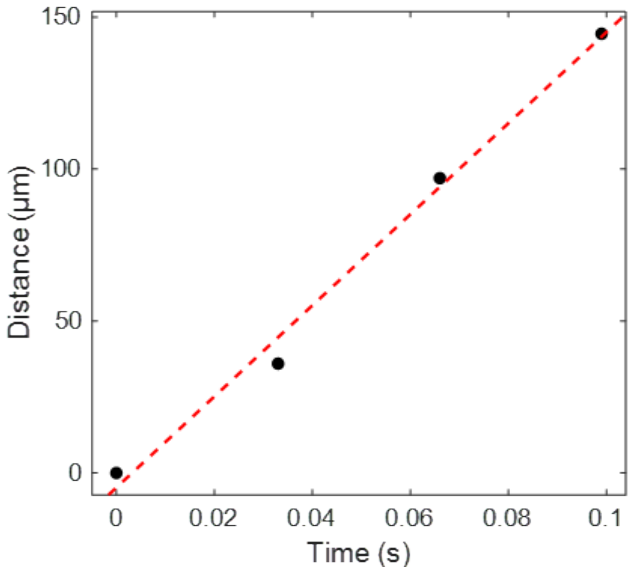

Figure S6: Time trace of the trajectory of a representative particle flowing in the microfluidic channel used to calculate the flow velocity. The red line is a linear fit to the data. The position of the trapped particle was taken as the reference.

S7: Positional Precision of Particle Manipulation in OHT

A custom-written MATLAB code was used to extract the position of the particle (centroid), from the image frames extracted from the Supplementary Video S10. Figure S8a and S8b are the representative frames showing the position of the trapped particle within the channel at optical power of 182 mW and 500 mW, respectively. The flow velocity was maintained constant in the channel. The position of the trapped particle, while the particle was manipulated multiple times between the two position is shown in Figure S8c. The mean positions of the trapped particle for all the iterations were used to calculate the accuracy of particle manipulation by OHT.

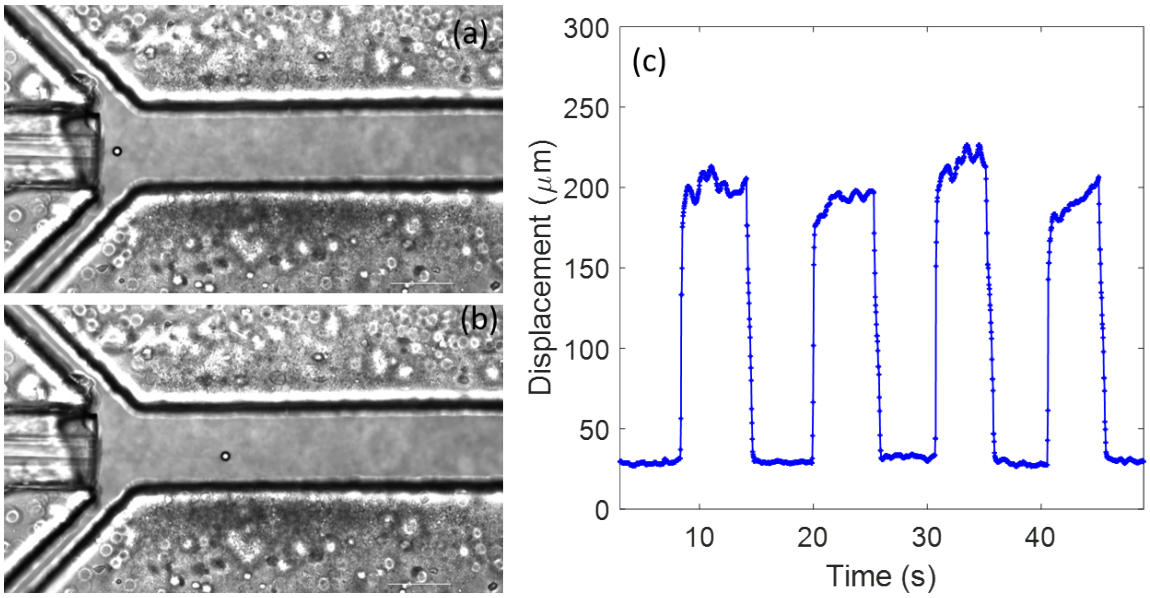

Figure S7: Microscope image showing the position of a 15 µm polystyrene particle trapped using OHT at fiber laser power of (a) 182 mW and (b) 500 mW. (c) The position of the trapped particle along the X-direction, as the particle is manipulated multiple times between two positions in the channel by alternating between two laser powers.

S8: Opto-hydrodynamic Tweezers Chip Assembly

The microfluidic device is fabricated by standard soft lithography [5]. A PDMS slab consisting of the fluidic channels is permanently bonded to a 50x75mm cover glass of a no.1 thickness (130-160µm) after the exposure to oxygen plasma. Next, the cleaved and cleaned PM photosensitive single mode optical fiber ($OD_{cladding}$=125±1µm) is inserted to the bonded chip through a dedicated channel of which one end is connected to the fluidic network and the other end is left open to the surroundings. The channel designed for inserting the fiber has a tapered geometry (from the free opening towards the fluidic network) as shown in Figure S8 (encircled in red). The broad opening (channel width = 800 µm) of the fiber-guiding channel provides for easy insertion of the optical fiber and the subsequent tapered geometry for easy fiber guidance to the junction with the fluidic channels. The channel width of 125 µm at the final millimetres before the junction allows for a snug fit of the fiber in the channel, allowing for minimal error in positioning the fiber's tip. Note that the height of all of the channels (including the fiber-guide channel) is the same as the diameter of the cleaved fiber, i.e. 125 µm.

While securing the fiber in place with bare hands a small drop of acrylic resin-based UV adhesive (Drei Bond, Poland) is introduced at the open end of the fiber-guide channel (while the fiber is already inserted), which fills the empty corners of the fiber-filled rectangular channel through capillary action. The flow of the UV adhesive is monitored under a microscope. When its meniscus is just a few microns

away from the junction with the fluidic channels, an appropriate UV exposure is applied to initiate cross linking of the adhesive. While inexpensive pocket lamps, gel-nail lamps or dental curing lamps could be used, we used (and recommend to use) a somewhat more expensive high-performance precision gluing UV spot-gun (2000 mW/cm^2; SPOTcure 01, IST Metz, Germany) and 30s exposure time.

The insertion of the fiber itself requires no strict constraints. One needs to ensure that the fiber is laying on a flat surface at the same level as the insertion hole and is not inclined during insertion. Furthermore, proper measures must be taken to ensure the glue does not enter the main channel as this would clog the chip and make it unusable. However, this can be easily avoided with a proper selection of the UV adhesive's viscosity. We used a highly viscous glue (2200 cP) for which filling the fiber-guide channel takes a few minutes thus the flow of the glue can be stopped at a precise position calmly, without very precise timing. However, with a UV adhesive with around 500cP the filling would take around 10-20 seconds, which is still doable and speeds up the fabrication process.

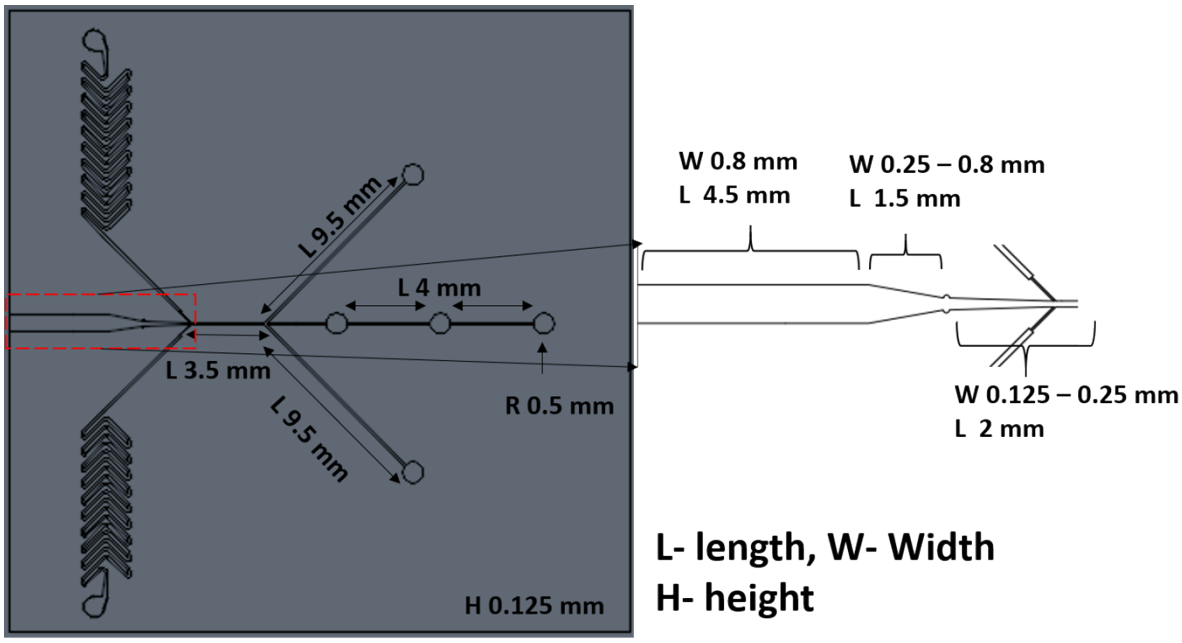

Figure S8: Depicts the CAD design of the OHT chip with dimensions. The dimensions for the fiber insertion channel are given on the right. The overall height of the chip is 125 µm.

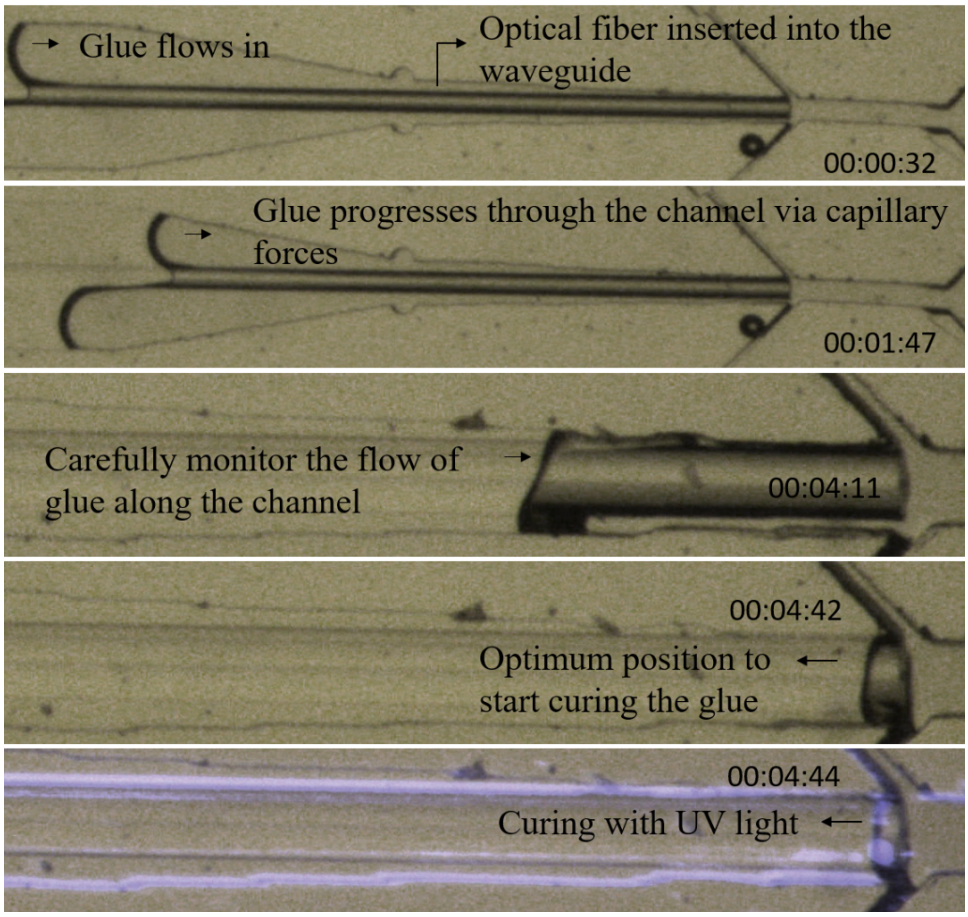

Figure S9: Time sequenced optical images demonstrating the gluing of the optical fiber within the microfluidic chip (Time depicted in hh:mm:ss format)

Supplementary Videos

Supplementary Video S1: 3D hydrodynamic flow focusing in a microfluidic channel.

Supplementary Video S2: Continuous trapping of single polystyrene particles with high efficiency and throughput in an OHT.

Supplementary Video S3: Simultaneous trapping of multiple polystyrene particles forming linear chains in an OHT.

Supplementary Video S4: Trapping of a single 15-µm polystyrene particle in an OHT.

Supplementary Video S5: Auto-alignment of particle trajectory by optical gradient force in OHT.

Supplementary Video S6: Trapping of particles of different sizes, shapes, and refractive indices, including mammalian cells, with OHT.

References

(1) Hsu, C.-H.; di Carlo, D.; Chen, C.; Irimia, D.; Toner, M. Microvortex for Focusing, Guiding and Sorting of Particles. *Lab Chip* **2008**, *8*, 2128–2134.

(2) di Carlo, D.; Edd, J. F.; Humphry, K. J.; Stone, H. A.; Toner, M. Particle Segregation and Dynamics in Confined Flows. *Phys Rev Lett* **2009**, *102*, 94503.

(3) di Carlo, D. Inertial Microfluidics. *Lab Chip* **2009**, *9*, 3038–3046.

(4) Zhao, Y.; Li, Q.; Hu, X. Universally Applicable Three-Dimensional Hydrodynamic Focusing in a Single-Layer Channel for Single Cell Analysis. *Analytical Methods* **2018**, *10*, 3489–3497.

(5) Xia Y, Whitesides GM. Soft Lithography. Angewandte Chemie International Edition. 1998 Mar 16;37(5):550–75.